SEVENTEENTH EUROPEAN ROTORCRAFT FORUM

Paper No. 91 - 37

ANALYSIS OF HELICOPTER ROTOR-FUSELAGE INTERFERENCE WITH TIME AVERAGED PRESSURE DISTRIBUTION

S.R. Ahmed, J. Raddatz
DLR, Braunschweig, Germany

W. Hoffmann
Technical University Braunschweig, Germany

September 24-27, 1991

BERLIN, GERMANY

Deutsche Gesellschaft für Luft- und Raumfahrt e.V. (DGLR)

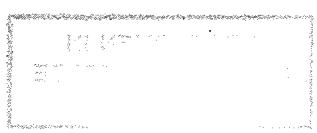

ANALYSIS OF HELICOPTER ROTOR-FUSELAGE INTERFERENCE WITH TIME AVERAGED PRESSURE DISTRIBUTION

S.R. AHMED, J. RADDATZ
German Aerospace Research Establishment (DLR)
Braunschweig, F.R.G.

W. HOFFMANN
Institute for Flight Mechanics, Technical University
Braunschweig, F.R.G.

Abstract

The aerodynamic interference between main rotor and fuselage of a helicopter is investigated experimentally with the help of time averaged pressures measured on the fuselage surface. A total of 450 pressure taps were distributed over the fuselage surface in regions where the interference effects were expected to be severe.

The facility used was a 1:6.5 geometrically scaled down model of BO 105 helicopter operated in open test section of DLR 3.25 m x 2.8 m subsonic wind tunnel in Braunschweig. The rotor of the model has a diameter of 1.5 m and is mach-scaled. Parameters varied are thrust ratio, advance ratio and fuselage incidence. Some global flow visualization with smoke filaments was also performed.

Symbols

c	Blade chord [m]
$c_p^* = 100(p-p_\infty)/(\frac{\rho}{2}\Omega^2R^2)$	Pressure coefficient nondimensionalized with rotor tip speed stagnation pressure
$c_T = T/(\rho\pi^2R^4)$	Thrust coefficient
Ma	Mach number
n	Number of blades
p	Time averaged static pressure [Pa]
p_∞	Tunnel free stream static pressure [Pa]
R	Rotor radius [m]
T	Rotor thrust [N]
V_∞	Tunnel free stream velocity [m/s]
α	Fuselage incidence [Deg.]
$\mu = V_\infty/(\Omega R)$	Advance ratio

Ω	Rotor rotational speed [rad/s]
ρ	Air density [kg/m^3]
$\sigma = nc/(\pi R)$	Rotor solidity

Introduction

Interest in the aerodynamic interaction between rotor and fuselage of a helicopter has grown steadily in the past years. This is due to the changing system requirements and operational doctrines. Consequently identification of interaction phenomena, understanding them and inhibiting their adverse effects have become areas of active technical investigation in research and industry. Need for improved operational economy and performance, reduction of vibratory loads, lesser pilot load through improvement of handling qualities, low internal and external noise etc. are some of the items warranting a deeper insight into the complex interaction mechanisms.

Since the main rotor operates in close proximity to the fuselage, major aerodynamic interactions occur between these components. The fuselage displaces the free stream flow whereby the angle of attack over the rotor disc is altered. Presence of the fuselage distorts the main rotor wake changing thereby the blade/vortex interactions. On the other hand the main rotor wake immerses the fuselage in an unsteady downwash. These phenomena are directly linked to the performance, vibratory loads, handling qualities and acoustics of the helicopter.

Numerical methods to predict aerodynamic interaction are currently in a research stage. Comprehensive analysis codes which can shorten the design effort remain an anticipation for the future. Presently they do not represent an alternative to wind tunnel or flight test. Flight tests with prototype flying machines are seldom used for basic research. Only wind tunnel tests with scaled models are suitable for detailed analysis and form the basis of current design practice. Such experimental results are also necessary to validate codes being developed.

This paper presents wind tunnel test results conducted with a mach- scaled rotor/fuselage model developed jointly by the Institute of Flight Mechanics, Technical University Braunschweig (TU-BS) and the German Aerospace Research Establishment (DLR). Rotor and fuselage are a 1:6.5 scaled down version of the BO 105 helicopter. Model rotor diameter is 1.5 m and in the current version of the fuselage, tail boom and empennage are not simulated.

Past work with model rotors has shown that reliable data can be obtained if careful attention is paid to scaling laws (Ref. [1] to [5]). Two comparable helicopter model test facilities of the type described here are the 2MRTS of the US Army, Ref. [6] and the one developed at the University of Maryland in US, Ref. [7].

The outstanding features of the TU-BS/DLR model are the hingeless rotor, patterned after the original BO 105 helicopter, and the high degree of dynamic fidelity of model blades with the full scale counterpart. This is desirable both for aerodynamic and flight mechanics investigations.

Model Details

Figs. 1a and b show the general arrangement of the model. It consists basically of a rotor drive system, rotor blades and a fuselage. The rotor drive system includes a hydraulic motor (101), a gear belt transmission (107, 108, 109), a slip ring assembly (111, 213), rotor control actuators (114) and a rotor shaft (31) mounted on a platform (1). The platform is suspended from the metric end of a six-component strain gauge balance (105) which is used to measure rotor loads; the other (ground) end of the balance is attached to the lip extension (8) of the model support sting (12). A second six-component cylindrical strain gauge balance (106), Fig. 1b, mounted parallel to the fuselage axis from side edge of the sting lip, supports the fuselage shell. Simultaneous measurement of the individual rotor and fuselage loads is thus possible.

Oil under pressure is supplied to the hydraulic drive motor from a indigenous unit outside the model. The pressure oil circuit consists of steel pipe (18, 19) running through the hollow sting. The rotor drive system consists of a 16 kW hydraulic motor driving a rotor shaft through a gear belt transmission. The rotor hub is modelled after the hingeless rotor design of BO 105 helicopter with four rotor blades. It could not, however, be geometrically scaled to the original and is oversize. For a correct simulation of blade root loads, mast moments and rotor natural frequencies, an accurate radial positioning of blade securing bolts corresponding to that of BO 105 rotor was realized.

The rotor control system uses three electromechanical actuators (114) to position a swash plate that determines collective and cyclic control of the rotor blade pitch. A mini computer (Hewlett-Packard Micro 24) converts the blade pitch input values into position signals for the acutators. A fully computer controlled trimming of rotor for given thrust values is under development.

Rotor hub arms are machined integrally with the rotor shaft (31). Instrumentation is provided on the hub and rotor blades to allow instantaneous real time monitoring of blade motions, bending and torsional stresses and push rod loads. The data is transmitted with a 24-channel slip ring assembly (111) installed on the rotor shaft on to the fixed system.

The rotor blades are of rectangular planform, 5 mm thick and have a chord of 42 mm, Fig. 2. Blade profile and structure is identical to the full scale counterpart, resulting in similar rotor characteristics. The geometric characteristics of the rotor are summarized in Table 1.

Table 1: Rotor geometry

Number of blades, n	4
Rotor Radius, R	0.75 m
Blade chord, c	0.042 m
Rotor solidity, σ	0.071
Blade twist (linear)	-6°
Airfoils	NACA 23012

The fuselage shell is mounted independently from the rotor system and may be configured to represent any desired shape consistent with the requirement to have adequate internal clearance to avoid contact with any internal parts or the support sting. The base line configuration is a geometrically 1:6.5 scaled down version of BO 105 fuselage without tail boom and empennage. The shell is fabricated from fiberglas reinforced plastic and is mounted to the outer casing of a six-component cylindrical stub balance. For easy access to the drive system and other internal components, the shell is made of two halves joined together with a row of screws in the plane of symmetry.

For pressure measurements, 450 pressure taps were arranged on the starboard and port sides of fuselage surface to investigate the expected flow asymmetry. These pressure acquisition points were distributed over 4 vertical (x=constant) and 10 horizontal (z=constant) fuselage sections, as shown in Fig. 3. Moreover two rows of pressure taps, lying on either side of plane of symmetry (y=0) were provided. A more comprehensive description of the model is available in [8].

Wind Tunnel Facility and Test Set-Up

The tests were performed in the DLR subsonic wind tunnel at Braunschweig. This facility, described in Ref. [9], is an open test section closed return wind tunnel with a 3.25 m by 2.8 m nozzle with a working section length of about 5.7 m. Maximum continuous wind speed in the open test section is 75 m/s and turbulence intensity in the empty test section lies below 0.15%. All tests were conducted at rotor blade tip speed of 220 m/s and the advance ratio changed by varying the free stream velocity.

The configuration tested was the 4 bladed rotor and the BO 105 helicopter fuselage without tail boom and empennage. An approximate simulation of the tail boom is effected through the model support sting as explained below. Fuselage overall dimensions are: length = 0.682 m; width = 0.23 m and height = 0.321 m. Spacing between rotor cowl top surface and rotor plane was constant and equal to 0.055 m. Different shells identical in their geometry were used for pressure distribution measurements and flow visualization to avoid fouling of pressure taps and tubing.

The pressure taps from fuselage shell were connected to a bank of Scanivalve electromechanical pressure switches using lengths of vinyl tubing. The tubing was pasted flush on the inner side of the fuselage shell and routed along the support sting on to the Scanivalves arranged atop the support arc.

General arrangement of the test set-up is to be seen in the photographs of Fig. 4a, b. The model is installed at the upstream end of a hollow support sting; the downstream end of the sting is clamped in a housing at the top end of a stiff circular arc, which in turn is mounted in a vertical plane to a turnable platform on the ground. The arc segment can be continuously extended out of a guide casing to effect model (rotor and fuselage in unison) incidence. At zero incidence, the support sting axis lies 3.5 m above the ground and coincides with the tunnel axis.

Test Spectrum

The results presented here were obtained in the framework of tests designed to assess the effect of rotor thrust, advance ratio, and fuselage incidence on the time-averaged pressure distribution over the fuselage surface.

Data were obtained in hover and forward flight for the isolated fuselage and the rotor/fuselage configuration. For the isolated fuselage tests, the rotor blades were removed and data measured with the hub stationary with hub arms fixed at 45° azimuth angle. This data served as a baseline to analyse the aerodynamic interaction between rotor and fuselage. Table 2 indicates the range of parameter variation performed in the tests.

Table 2: Range of test parameters

Parameter	Test Values
Advance ratio μ	0; 0.075; 0.15
Wind speed V_∞	0; 16.5; 33 [m/s]
Fuselage incidence α	0; 2°; 5°; -2°; -5°
Rotor thrust T	206; 542 [N]
Rotor speed	2800 [rpm]
Rotor tip Mach Number	0.65

In all tests, first the rotor speed was steadily increased quickly crossing the critical frequencies. Thereafter the collective pitch was adjusted to attain approximately the targeted thrust value. Wind speed was increased in small steps at the end of which the rotor was trimmed with longitudinal and lateral cyclic pitch inputs. This was continued till the desired advance ratio and thrust values were attained. Rotor speed was maintained at 2800 r.p.m. throughout the tests.

Test Results

From the large amount of data collected only a representative sampling is presented here. The analysis is based on time-averaged static pressure data for hover and forward flight. Parameters varied are thrust coefficient C_T, advance ratio μ and fuselage axis incidence angle α.

The static pressure distribution is presented as pressure coefficients c_p^* which are pressures non-dimensionalized with respect to rotor tip speed. With this definition of pressure coefficients, which is independent of tunnel wind speed, hover and forward flight conditions can be conveniently compared with one another. To facilitate rapid processing of the results the c_p^* values are plotted over equidistant abscissa intervals; these do not correspond to the actual abscissa coordinates of the pressure taps.

It can be seen from Fig. 5 that the increased dynamic pressure below the rotor causes a significant rise of the pressure level over the top and bottom of the fuselage as the rotor thrust is increased. Baseline configuration here is the isolated fuselage.

Major pressure rise occurs on the canopy with increase in rotor thrust. Apparently the fuselage bottom is affected almost over its entire length by the skewed rotor downwash. The underpressures are reduced considerably with increasing rotor thrust. In the base region (tap nos. 26 to 34), a noticeable pressure recovery occurs which can lead to a reduction of fuselage pressure drag. Fig. 6 shows the influence of rotor thrust on the pressure distribution of the starboard side (St.B.) in two horizontal sections H2 and H3 of the fuselage. The whole starboard side surface experiences a pressure rise whose magnitude increases with rotor thrust. Fuselage side surface is immersed in the skewed rotor downwash leading to this pressure rise. Also plotted in Figure 6 is the corresponding pressure distribution for the port side (Ps) indicating minor differences between the pressure on the two sides of fuselage surface. This shows that this particular fuselage configuration experiences no significant yawing moment.

Besides the behaviour of pressure increase with increasing thrust, the distribution for section H6 is different for the starboard and port side as seen in Fig. 7. With the pressures on starboard side being higher than on the port side, this may generate side forces and a rolling moment for the fuselage. The asymmetric pressure distribution is also of interest for powerplant intake location. Similar trend of pressure rise with rotor thrust is also exhibited in the sections H9 to H12. However, different behaviour of starboard and port side, is here not noticeable. For the sake of clarity, these data have not been plotted in the lower part of Fig. 7.

The effect of thrust increase on the pressure distribution in vertical sections Q2 and Q3 is demonstrated in Fig. 8. As noted

above the pressure rise with increasing thrust is also apparent here as well as the near symmetry of the distributions on starboard and backboard sides.

The influence of advance ratio on the pressure distribution is investigated in Fig. 9. For hover, positive pressures are generated on the top side (tap nos. 4 to 25) and negative to ambient pressures on the bottom side in section V1. With increasing advance ratio, the characteristics of fuselage flow become more and more dominant; the flow deceleration in the stagnation region and in front of cowl and acceleration on canopy top lead to corresponding high pressure peaks and a low pressure trough on the top side of fuselage contour. Low pressure peaks generated at points of strong curvature in front and rear part of bottom fuselage contour are also clearly visible for the higher advance ratio of μ=0.15. It is clear from this result that for high speed flight, fuselage main body flow characteristics are important. It is interesting to note that positive pressures prevail on the bottom surface of the rear end - at least in section V1 - for the forward flight conditions. Pressure distribution for hover bears no similarity to the forward flight results in section V1.

The situation in horizontal sections H2 and H3 (starboard side) shows similar variation with increasing advance ratio whereby negative pressure peaks (tap nos. 4 to 16 and 5 to 17) are seen in front and rear at points of strong contour curvature (Fig. 10). Comparison with corresponding distribution for the port side (not shown) for low advance ratio forward flight (μ=0.075) show some difference in rear end vicinity. For the higher advance ratio of μ=0.15 this asymmetry disappears.

In the upper most horizontal section H6 (Fig. 11) a drastic change in pressure distribution from hover flight condition is observed for advance ratio μ=0.15. At the lower value of μ=0.075, except at the rear end, minor deviation from hover situation is noticeable. The starboard and port pressure distributions in this section are asymmetric indicating a slight roll and side force tendency for the fuselage.

Change of pressure in the sections H9, H11 and H12 with advance ratio exhibits a pressure recovery at fuselage rear end (tap nos. 3 to 5 and 4 to 8) compared to the hover condition. With increasing advance ratio, the fuselage rear end is immersed more effectively in the combined onset and skewed rotor downwash flow which is apparently the reason for the pressure rise in this area. In the cross sections Q2 and Q3 the advance ratio causes a general decrease in pressure level especially in the section Q2 at μ=0.15, Fig. 12.

To investigate the effect of incidence on the pressure distribution, the fuselage was tilted over a range of positive and negative incidence angles α. Referred to the situation at zero incidence, positive α reduces the pressures on the canopy and at bottom rear end surface; negative incidence on the other hand primarily affects the fuselage bottom surface as evidenced by the results of Fig. 13 for section V1.

Data for the horizontal section H3, plotted in Fig. 14 exhibits a sensitivity only for negative incidence; the level of pressure is lowered below that for $\alpha=0°$. The starboard and backboard side pressure distributions for $\alpha=-5°$ differ only slightly and no yaw moments are induced on the fuselage.

The situation in cross section Q2, as plotted in Fig. 15, shows for negative incidence ($\alpha=-5°$) a slight pressure increase on the upper and a decrease on the lower part of this fuselage section. Only the upper part is affected with positive incidence ($\alpha=5°$). Negative incidence induces, as this result shows, a stronger pressure change.

Flow Visualization

Visualization of the flow was performed with smoke filaments in the plane of symmetry. A rake, fed by a smoke generator, was clamped vertically to the rim of wind tunnel nozzle about 2 m ahead of the rotor disc. The smoke intensity and visibility become poor with wind speeds higher than about 25 m/s, so that most of the visualization tests were performed at lower speeds.

Fig 16 (a, b, c) shows the effect of rotor thrust (at constant advance ratio and incidence) on the global flow characteristics. At zero thrust (Fig. 16a) the flow is fairly parallel to the fuselage axis. The flow going over the rotor disc appears to be due to the negative twist in vicinity of blade tip. Tail boom and fin area are immersed in the low energy wake flow from fuselage rear end. With increasing thrust (Figs. 16b and c) the flow in the rear portion is drastically changed. Fig. 16b is qualitatively representative of climb and Fig. 16c of (near) hover flight conditions. The adverse flow conditions for the tail rotor and control surface region generated due to flow deflection by rotor and fuselage wake are clearly visible. As noted earlier the hover flow deviates strongly from forward flight situation.

The influence of advance ratio, investigated in Figs 16d, e and f is just the opposite to that shown in Figs 16a to c. With rotor thrust held constant, increasing the advance ratio makes the flow field more and more parallel to the onset flow. This means that in the high speed flight regime, the flow around the fuselage becomes increasingly similar to that of the fuselage and the rotor wake wholly immeres the tail boom, control surfaces and the tail rotor.

It is interesting to note that the smoke filaments appear to retain their identity even after passing through the rotor disc.

Conclusions

A 1.5 m rotor mach-scaled helicopter model was used to investigate the aerodynamic interactions between the rotor and fuse-

lage. The model consists of a 16 kW hydraulic motor driven rotor system, a four bladed hingeless rotor and a 1:6.5 geometrically scaled BO 105 fuselage.

Wind tunnel tests were performed with and without rotor to evaluate the effect of thrust, advance ratio and incidence on the time-averaged pressure distribution on the fuselage. Four hundred and fifty pressure taps were distributed in horizontal and vertical rows over the starboard and port side of the fuselage to provide detailed information on areas of interest on fuselage surface. Visualization of the flow with smoke filaments was also performed.

Results from the present study provide an insight into the many faceted and complex interaction phenomena. Some of the findings can be summarized as follows:

1. With increasing rotor thrust a significant increase in the pressure level over the top and bottom surface of the fuselage is generated. This reiterates the theoretical and experimental results of Ref. [7]. Major pressure rise occurs on the canopy front. Also the bottom surface over its entire length is effected. On the rear end surface a pressure recoverey occurs which can reduce the fuselage pressure drag.

2. Only the topmost surface area exhibits a pressure asymmetry for the BO 105 fuselage. The side and lower surface pressures differ insignificantly for the starboard and backboard sides.

3. With increasing advance ratio, the pressure distribution over the fuselage surface becomes more and more similar to that of the isolated fuselage. The inference is that for high speed flight the aerpdynamic characteristics of the isolated fuselage become important and aerodynamic optimization of fuselage can significantly improve helicopter performance. Pressure distribution for hover does not bear similarity to the forward flight condition.

4. With increasing advance ratio, the slight pressure asymmetry noticed on the top surface disappears; also the underpressures on the rear end are converted to overpressures.

5. Effect of fuselage (and rotor) incidence indicates a significant pressure sensitivity over the major portion of fuselage surface for negative α. Also the magnitude of the pressure change is higher for negative than for positive incidence angles.

6. Flow visualization results qualitatively support the observations made above.

Acknowledgement

The authors wish to thank Volkswagenwerk AG for providing the smoke generation equipment. Help from the staff of DLR subsonic wind tunnel which was supervised by Mr. W. Hastreiter is gratefully acknowledged.

This work was supported by a grant from German Ministry of Research and Technology (BMFT). Results presented were obtained in the framework of EEC funded BRITE/EURAM Project SCIA.

References

[1] Fradenburgh, E.A., "Aerodynamic Design of the Sikorsky S-76 Helicopter", Preprint No. 78-06, 34th Annual National Forum, American Helicopter Soc., Inc., May 1978.

[2] Balch, D.T., "Full-Scale Wind Tunnel Tests of a Modern Helicopter Main Rotor - Correlation With Model Rotor Test Data and With Theory", Preprint No. 78-03B, Proceedings of the 34th Annual National Forum, American Helicopter Soc.; May 1978.

[3] Keys, Ch.N.; MacVeigh, M.A.; Dadone, L. and McHugh, F.J., "Considerations in the Estimation of Full-Scale Rotor Performance From Model Rotor Test Data", Proceedings of the 39th Annual Forum of the American Helicopter Society, May 1983, pp. 34-43.

[4] Ormiston, R.A., "Helicopter Modelling", Aeronautical Journal, Nov. 1973.

[5] Simons, I.A., "Test Facilities for Helicopters", The Aeronautical Journal of the Royal Aeronautical Society, Vol. 74, July 1970.

[6] Phelps, A.E. and Berry J.D., "Description of the U.S. Army Small-Scale 2-Meter Rotor Test System", NASA TM 87762, 1987.

[7] Leishman, J.G.; Bi, N.; Samak, D.K. and Green, M., "Investigation of Aerodynamic Interactions between a Rotor and a Fuselage in Forward Flight", American Helicopter Society 45th Annual Forum, Boston, MA, May 1989.

[8] Ahmed, S.R., Meyer, F.W., "A Mach-Scaled Powered Model for Rotor-Fuselage Interactional Aerodynamics and Flight Mechanics Investigations", Proceedings of the International Technical Specialists' Meeting on Rotorcraft Basic Research, March 1991, Georgia Institute of Technology, Atlanta, USA.

[9] Kausche, G.; Otto, H.; Christ, D. and Siebert, R., "Der Niedergeschwindigkeitswindkanal der DFVLR in Braunschweig (Stand 1988)", DFVLR-Mitteilung 88-25, 1988.

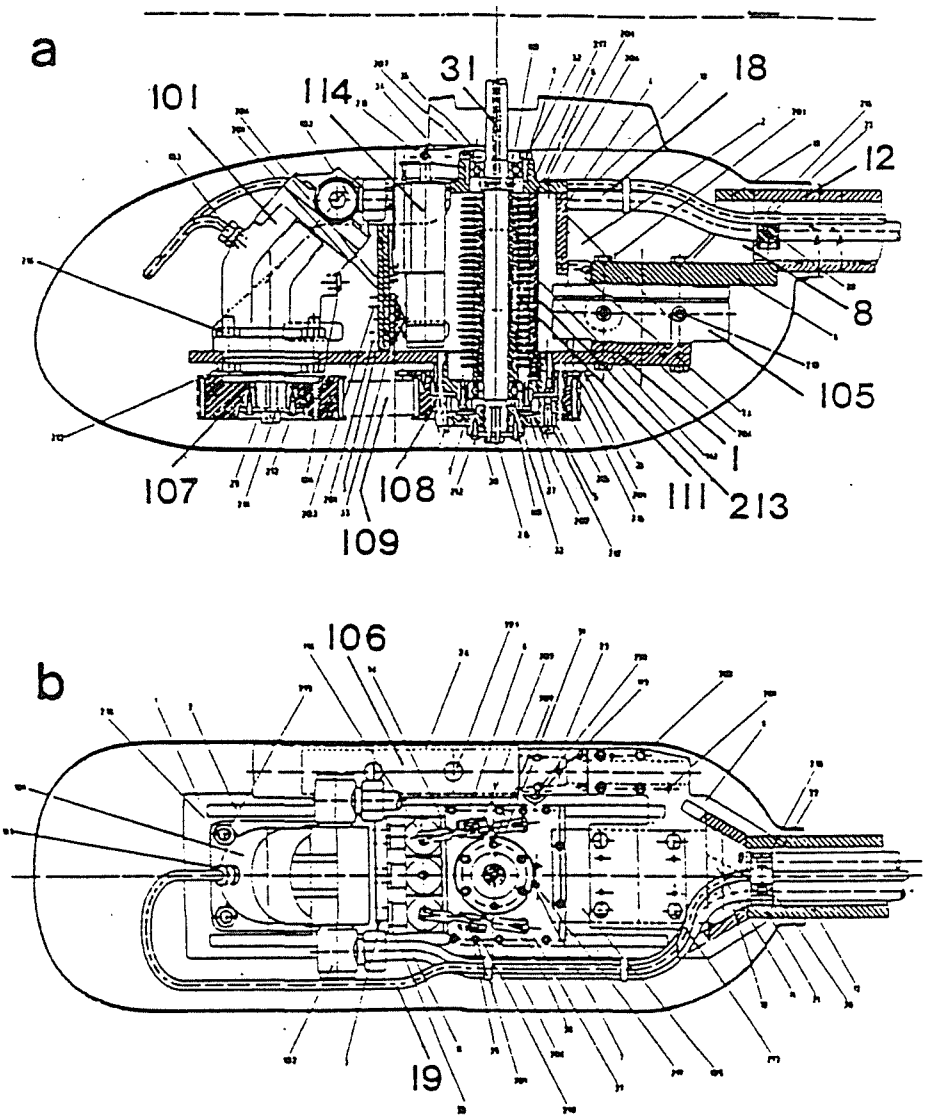

Fig. 1a,1b General arrangement of model components

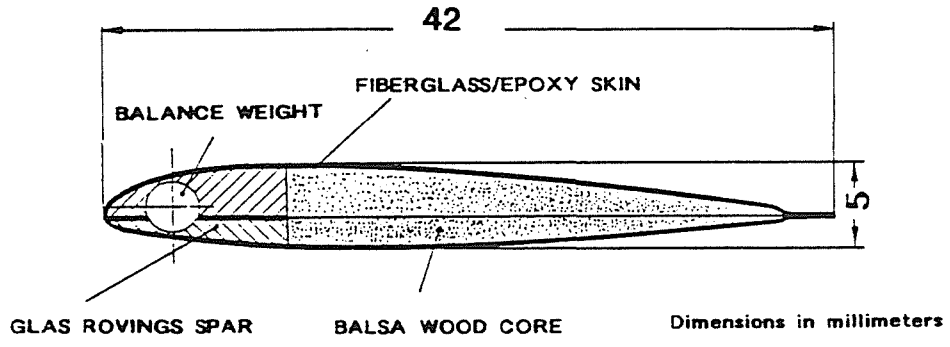

Fig. 2 Blade construction details

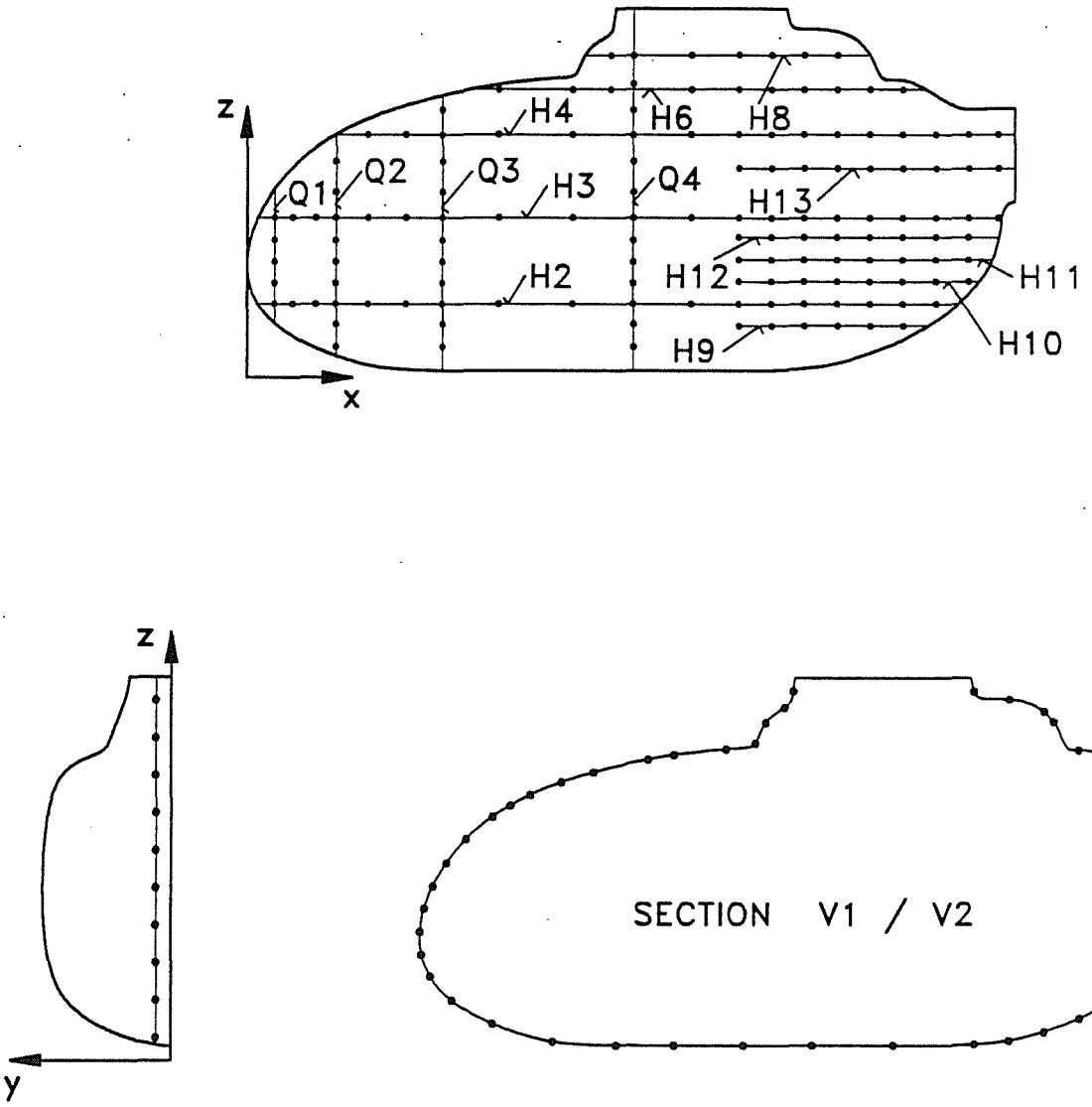

Fig. 3 Location of pressure taps on fuselage surface

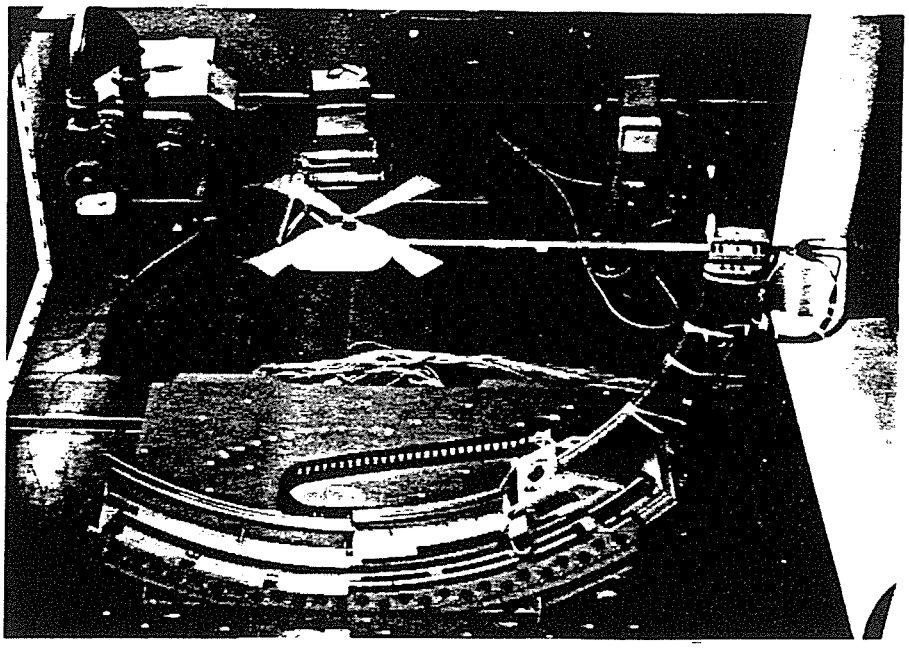

Fig. 4a Helicopter model mounted in DLR 3.25 x by 2.8 m subsonic wind tunnel

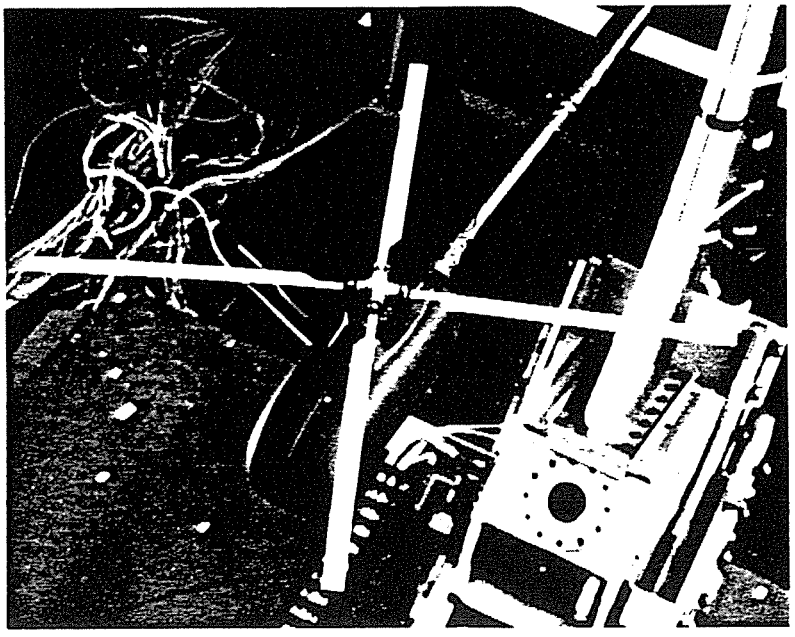

Fig. 4b Close-up view of model with flow visualization shell

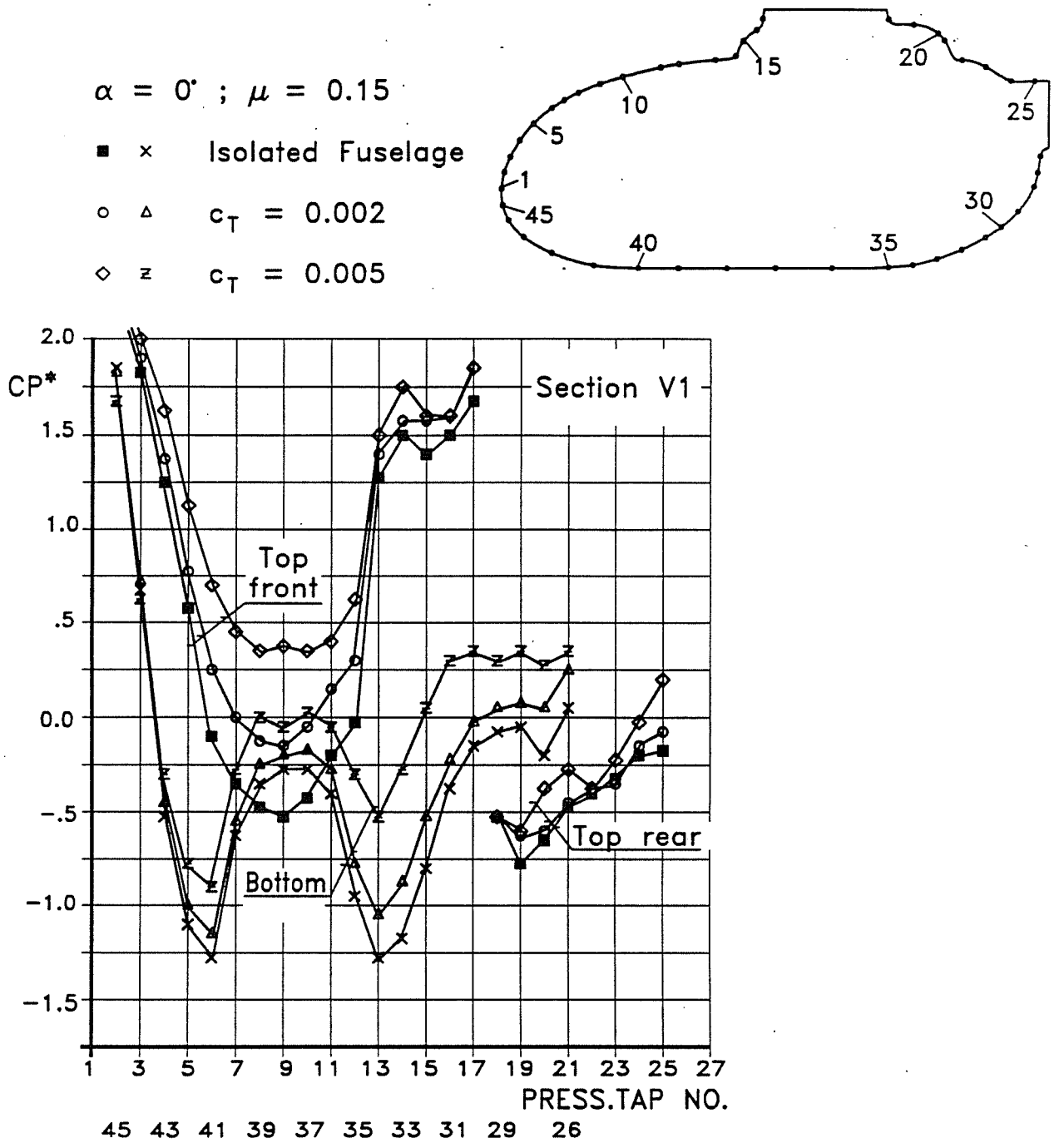

Fig. 5 Influence of rotor thrust on fuselage surface pressure distribution (Section V1)

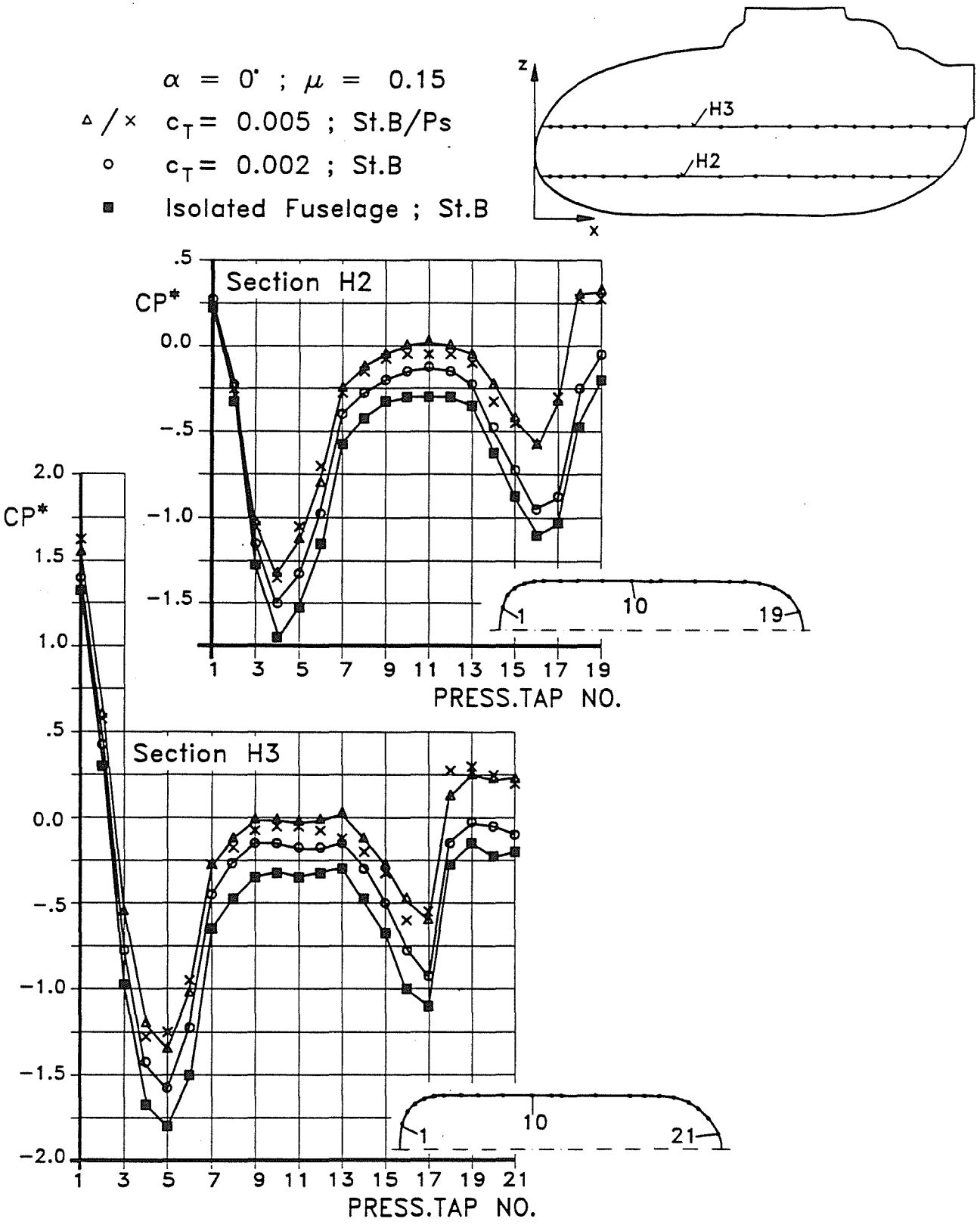

Fig. 6 Influence of rotor thrust on fuselage surface pressure distributions (Sections H2, H3)

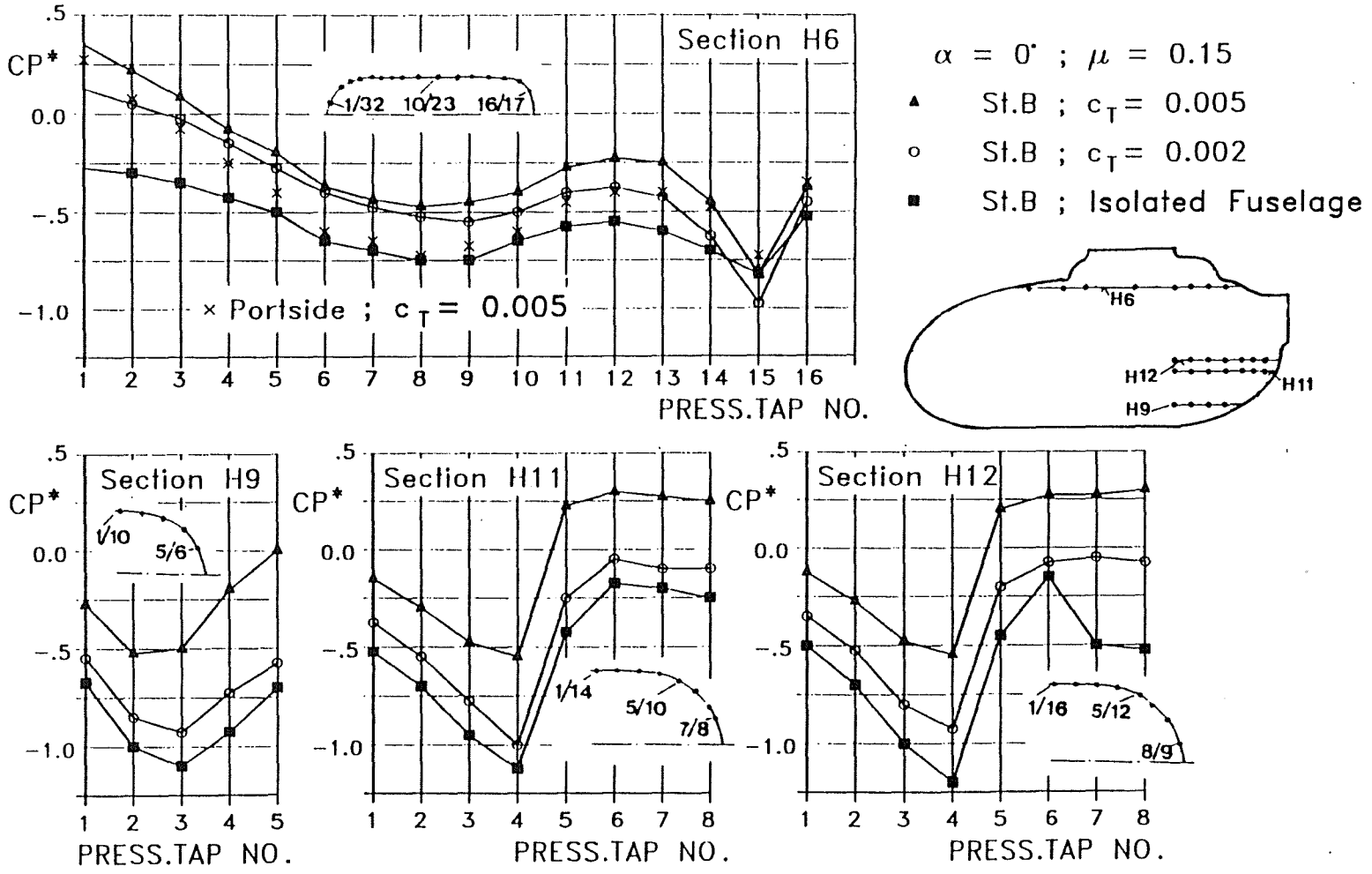

Fig. 7 Influence of rotor thrust on fuselage surface pressure distribution (Sections H6, H9, H11 and H12)

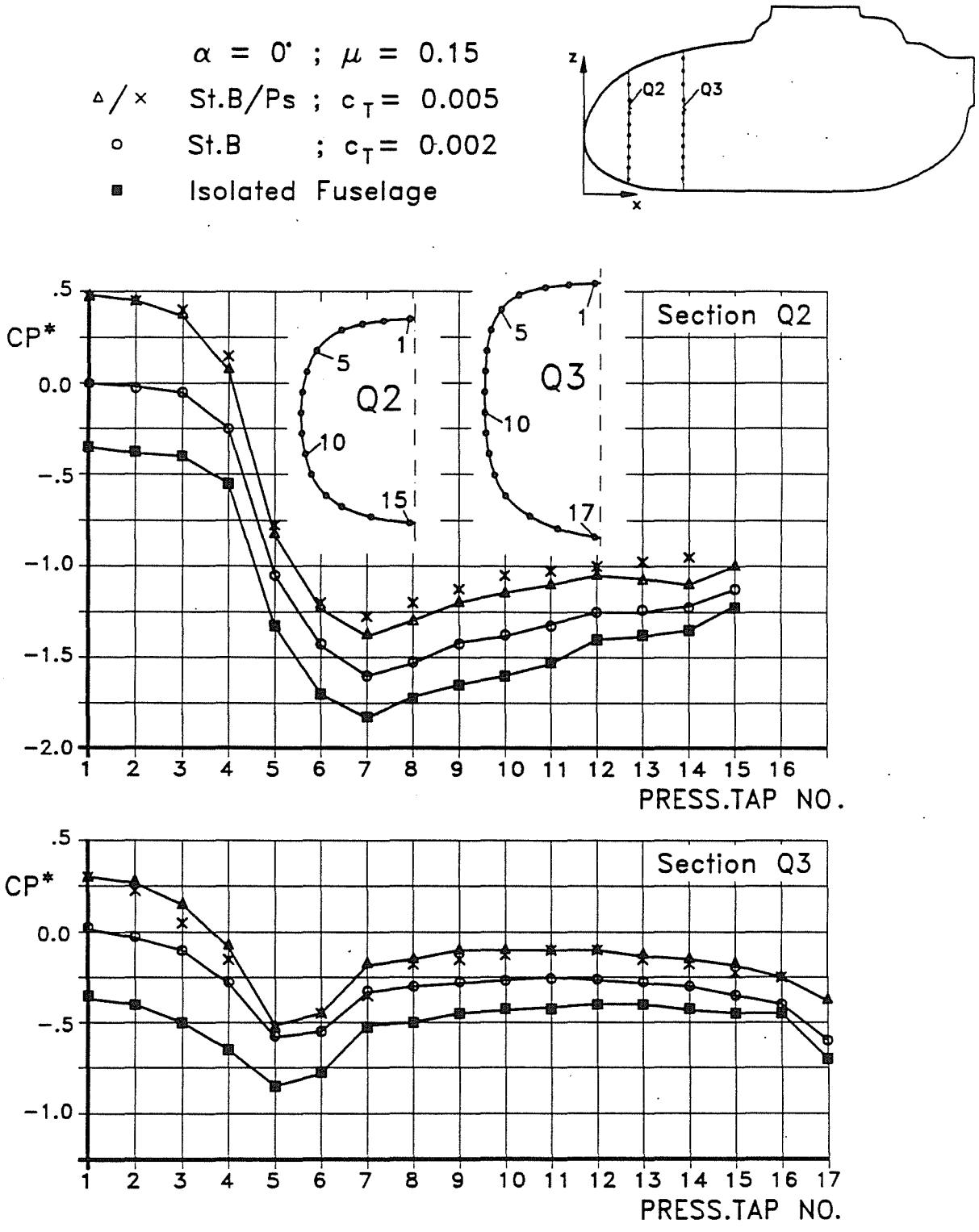

Fig. 8 Influence of thrust on fuselage surface pressure distribution (Sections Q2, Q3)

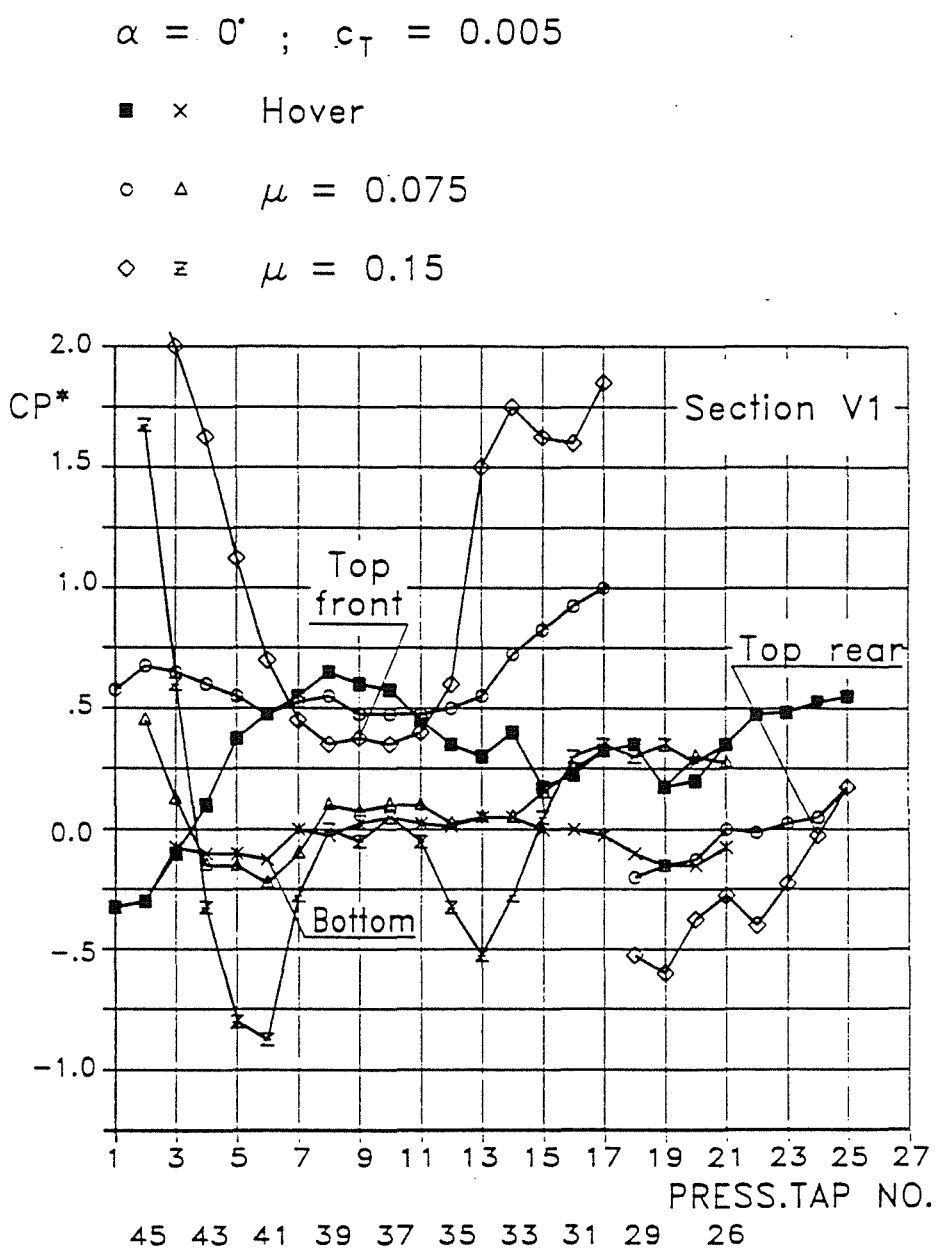

Fig. 9 Influence of advance ratio on fuselage surface pressure distribution (Section V1). See Fig. 5 for legend

$\alpha = 0^{\circ}$; $c_T = 0.005$

■ Hover ; St.B

○ $\mu = 0.075$; St.B

△ $\mu = 0.15$; St.B

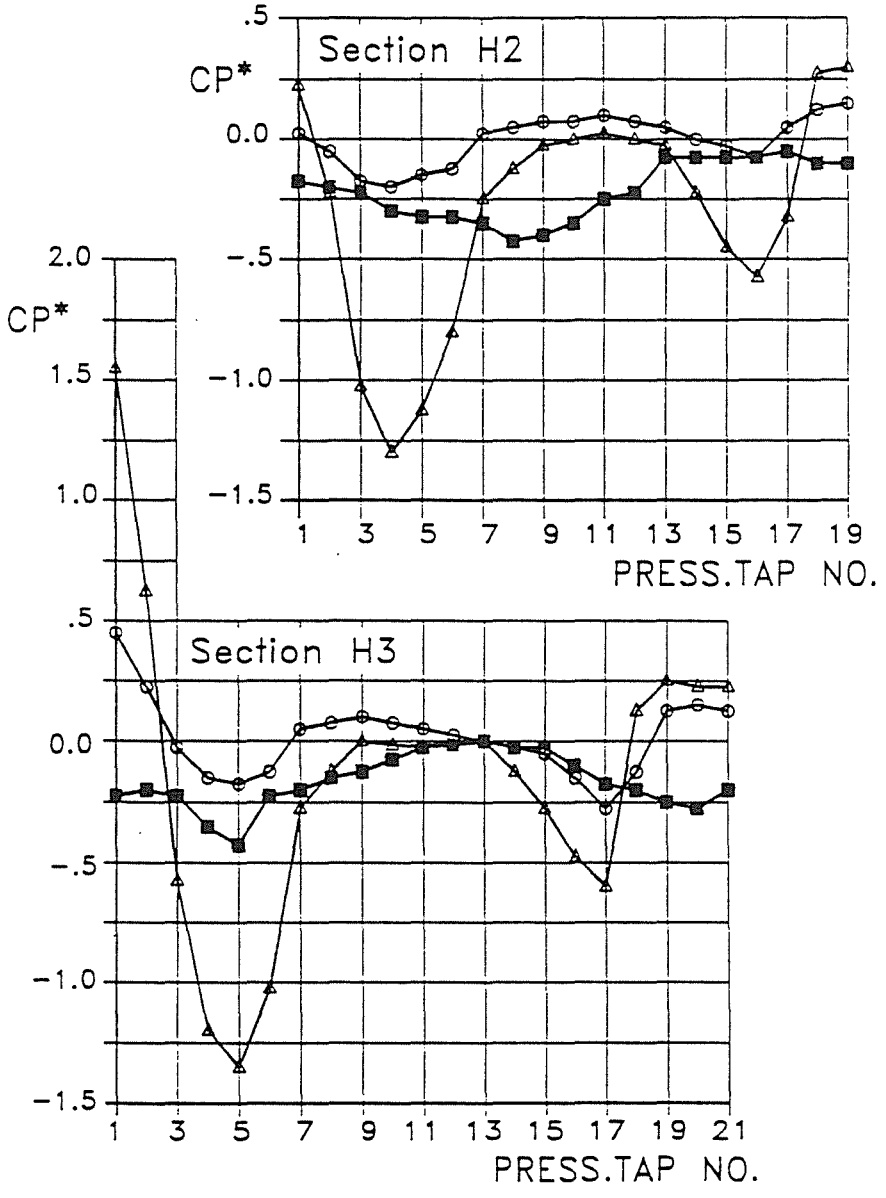

Fig. 10 Influence of advance ratio on fuselage surface pressure distribution (Section H2 and H3). See Fig. 6 for legend

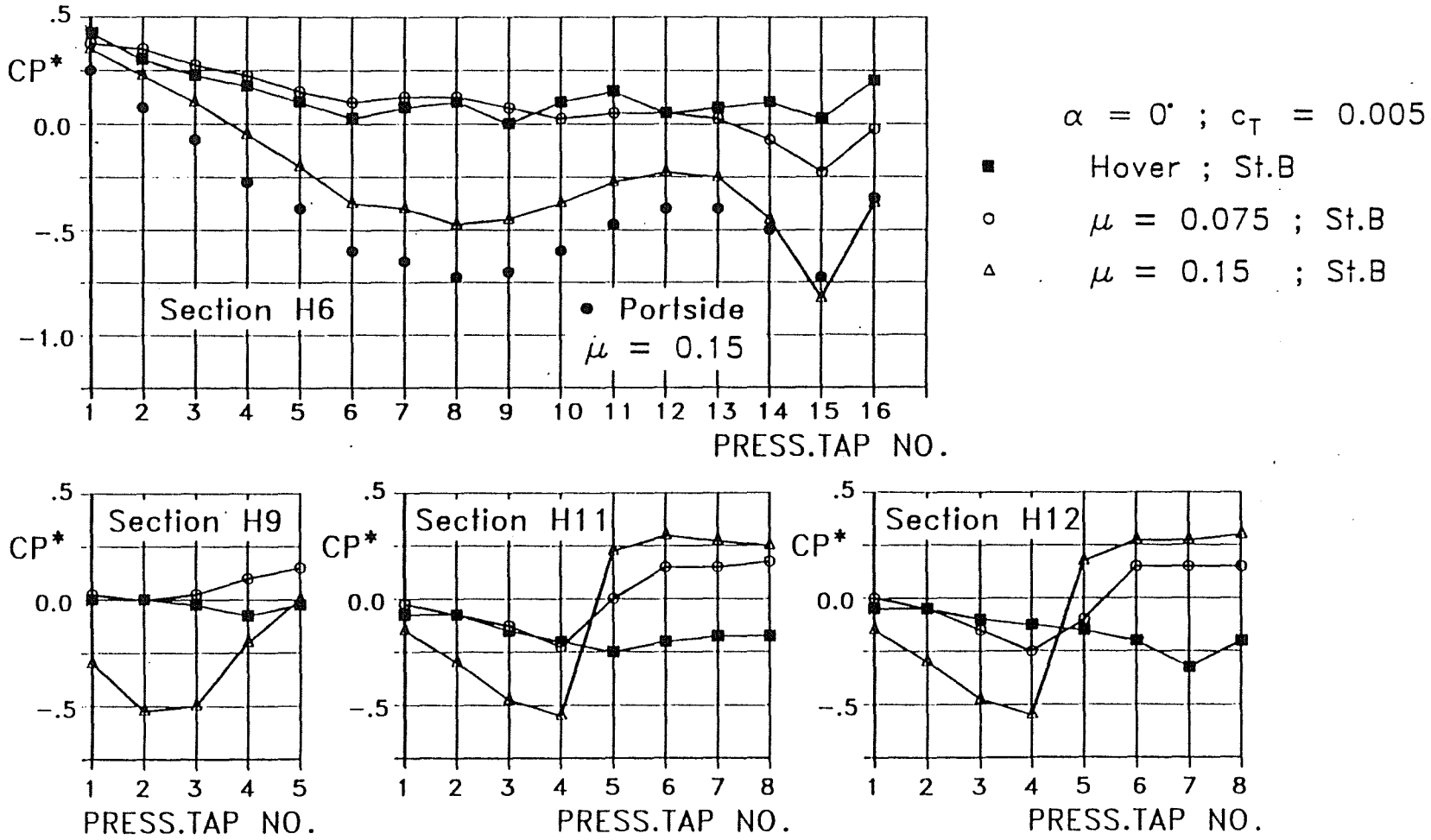

Fig. 11 Influence of advance ratio on fuselage surface pressure distribution (Sections H6, H9, H11 and H12). See Fig. 7 for legend

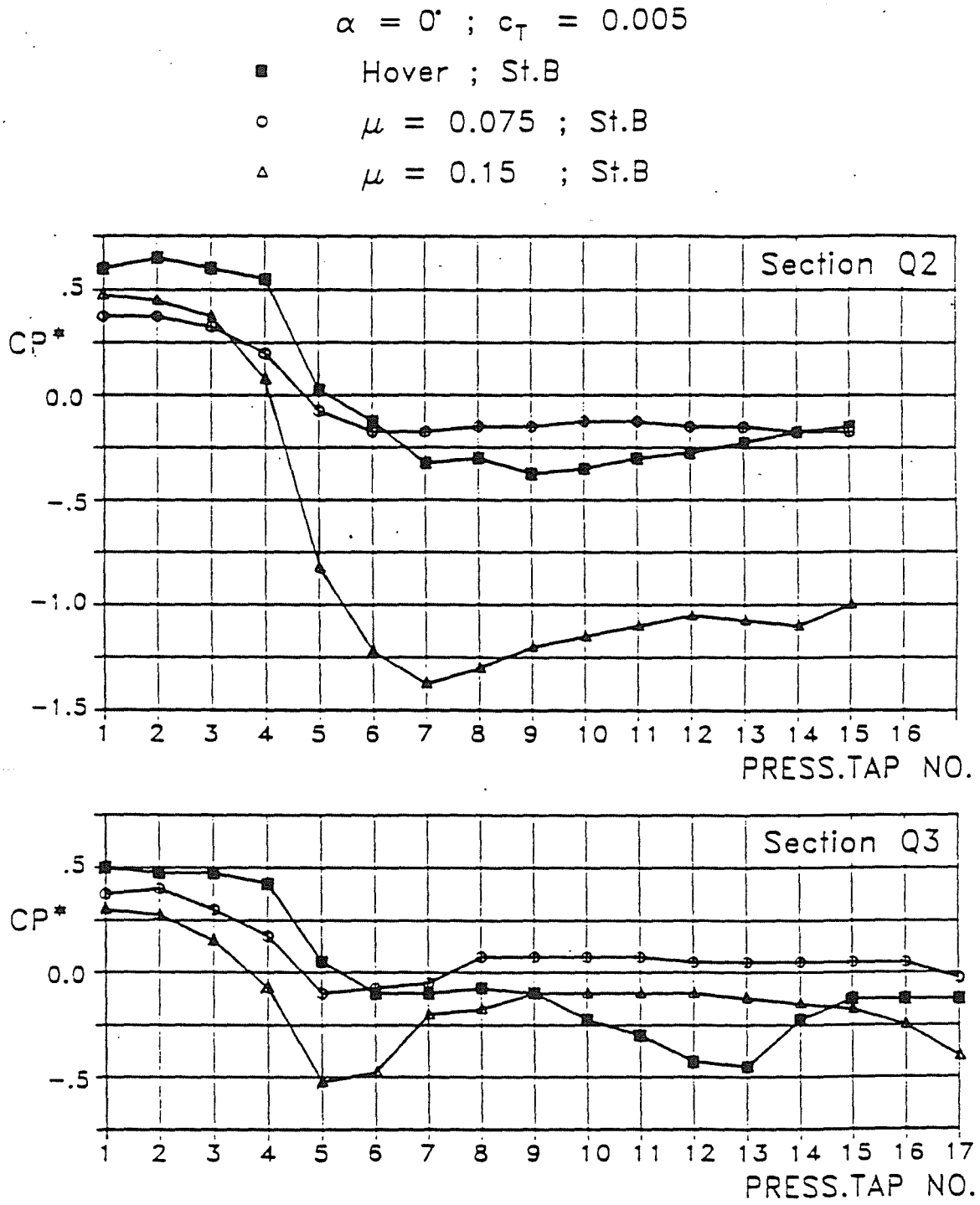

Fig. 12 Influence of advance ratio on fuselage surface pressure distribution (Sections Q2, Q3). See Fig. 8 for legend

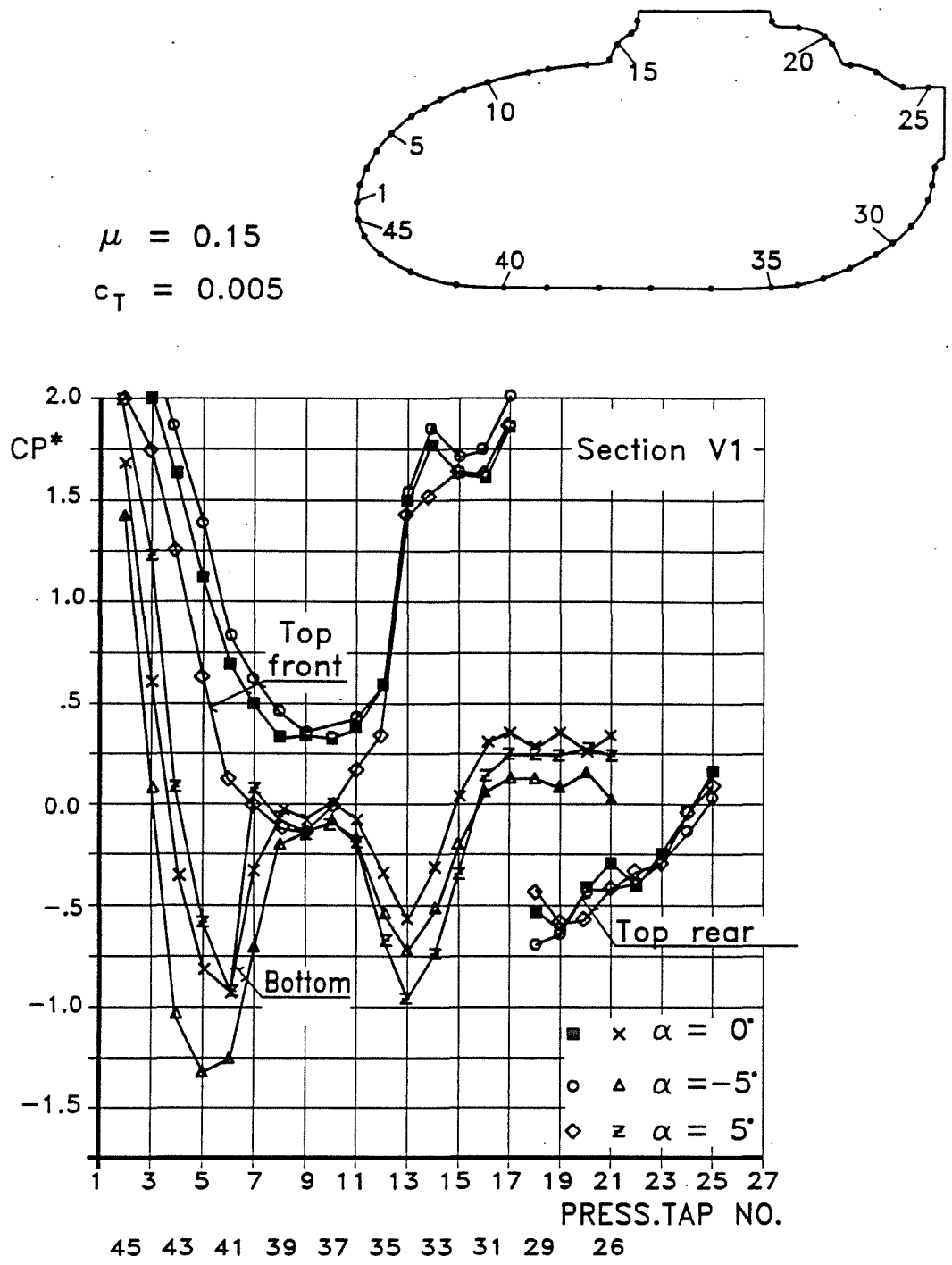

Fig. 13 Influence of incidence on fuselage surface pressure distribution (Section V1)

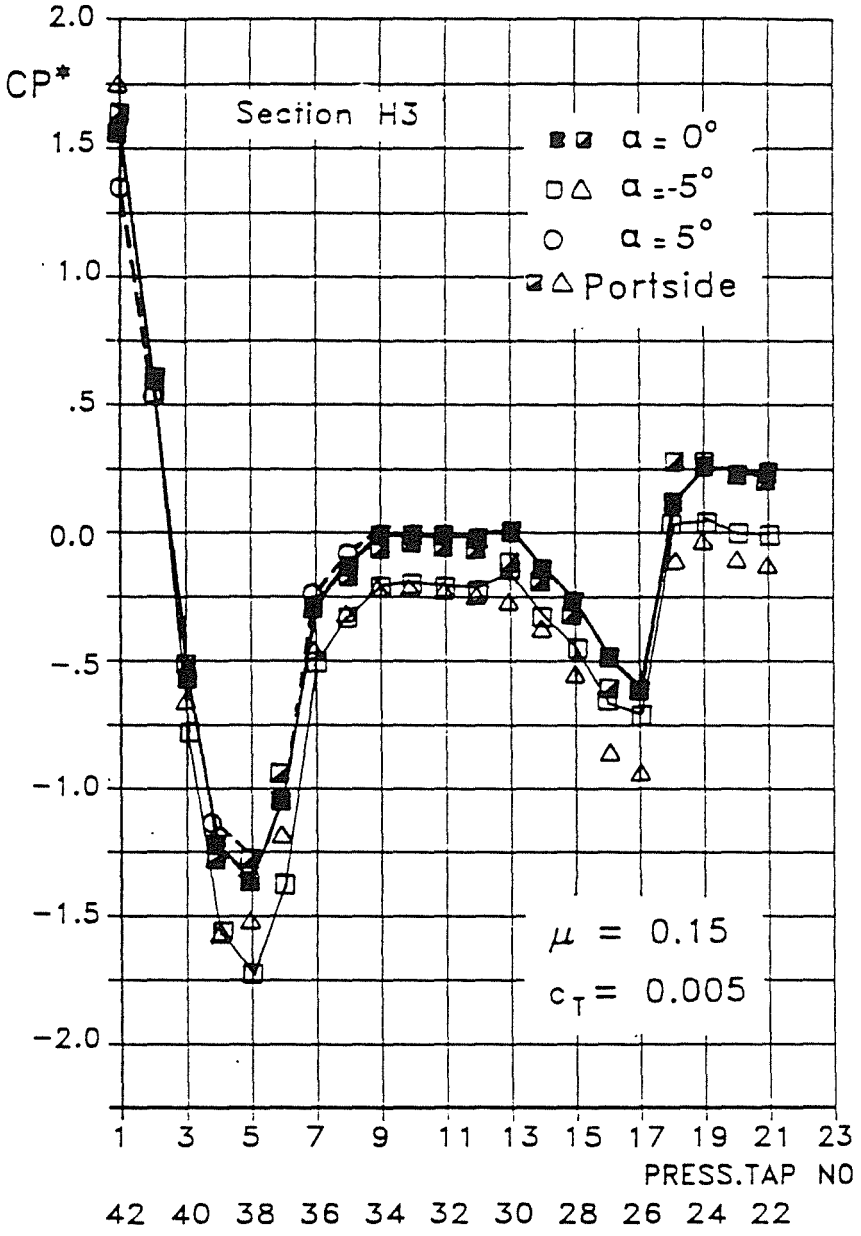

Fig. 14 Influence of incidence on fuselage surface pressure distribution (Section H3). See Fig. 6 for legend

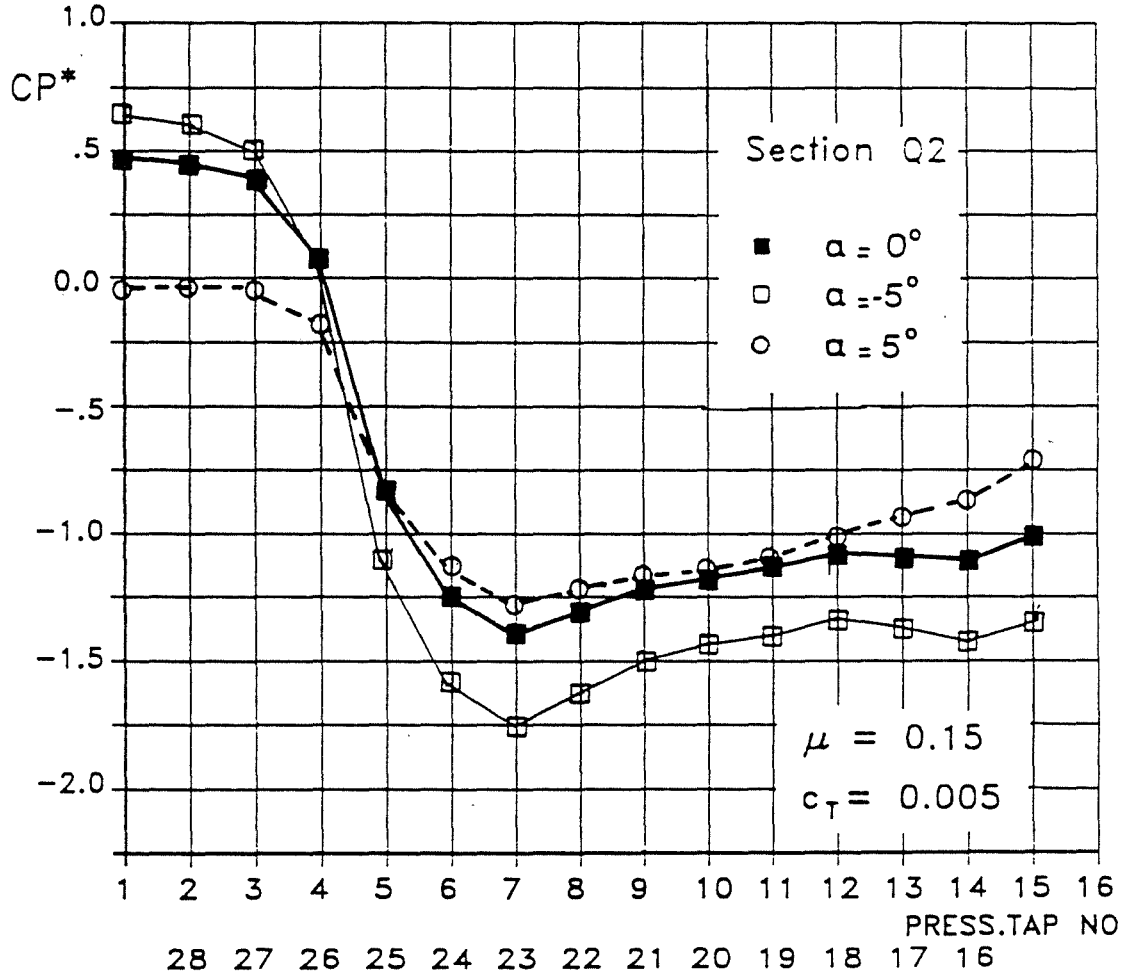

Fig. 15 Influence of incidence on fuselage surface pressure distribution (Section Q2). See Fig. 8 for legend

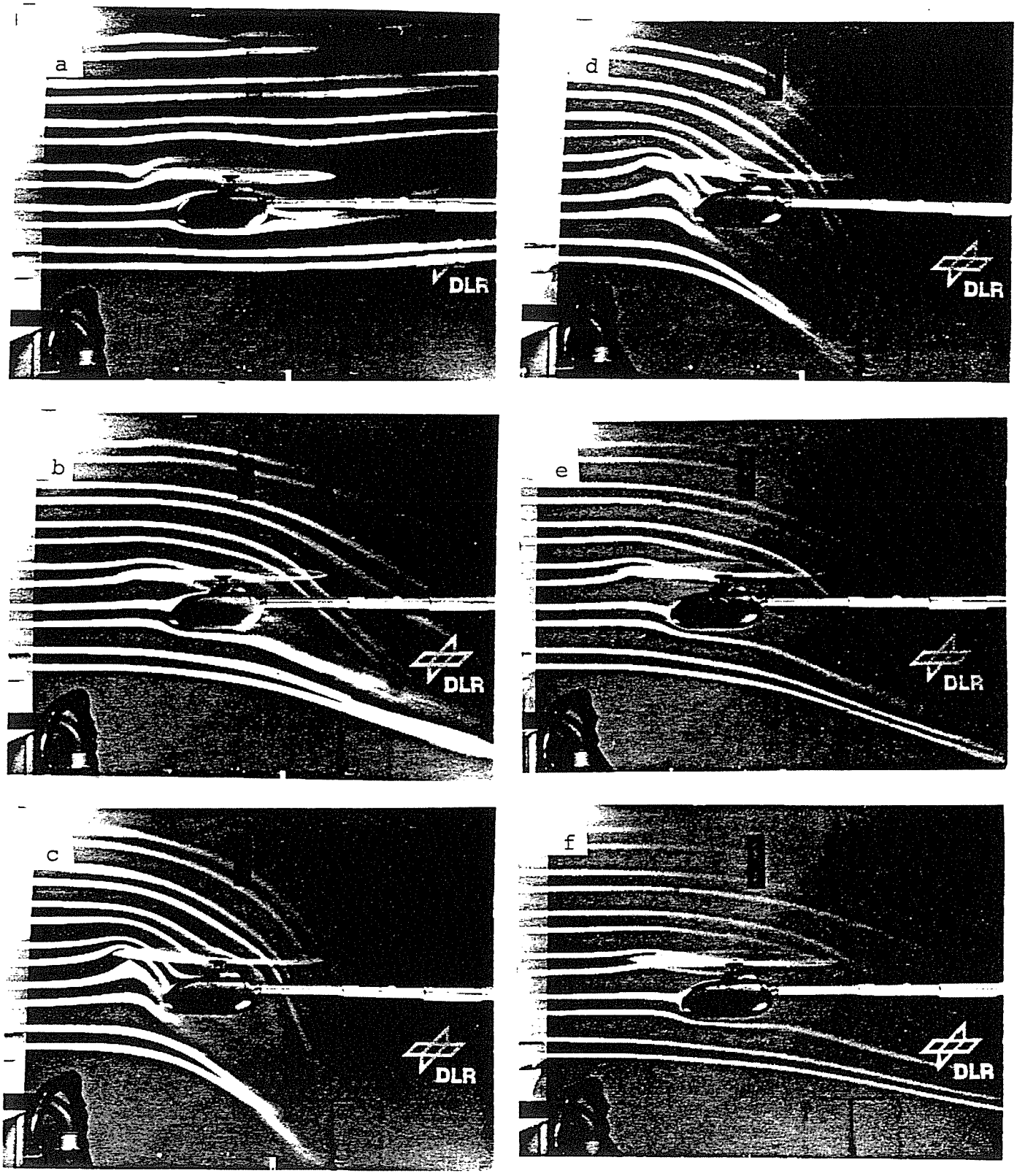

Fig. 16 Influence of thrust on flow
a) $c_T = 0$; b) $c_T = 0.002$; c) $c_T = 0.005$
a,b,c) $\mu = 0.05$

Influence of advance ratio on flow
d) $\mu = 0.025$; e) $\mu = 0.075$; f) $\mu = 0.10$
d,e,f) $c_T = 0.005$